MODELING OF THE PULLOUT TEST THROUGH THE CELL METHOD

Elena Ferretti
DISTART – Scienza delle Costruzioni, Faculty of Engineering,
Alma Mater Studiorum – University of Bologna, ITALY

Abstract

The Cell Method (CM) code with automatic remeshing for crack propagation analysis [6] is here used for modelling the pullout test. Particular emphasis is given to the analysis in the Mohr-Coulomb plane, since previous numerical models were not decisive in describing failure mechanism in pullout tests. The interpretations of experimental and analytical studies vary widely, and none of the existing explanations offer a complete description of the progressive failure of the concrete medium [21]. Nor do most existing interpretations appear to be totally compatible with the experimental evidence.

Analysis of the failure mechanism for the pullout test requires a failure criterion accurately describing crack initiation in tension loading. The Mohr-Coulomb criterion of the first code [6] has therefore been abandoned in favour of a more realistic criterion for the tensile state of stress, the Leon criterion.

The failure analysis has been performed for several ratios between the counterpressure diameter and the stem length (Fig. 1). Moreover, the complete crack path has been obtained for the geometry of the Lok-test. The evolving state of stress-strain for the Lok-test is also provided. The identification of the directions of principal stress completes the stress analysis. Modelling is performed both on the concrete specimen and on the steel insert, showing how the CM can easily handle domains with several materials.

Keywords: Cell Method, automatic remeshing, failure mechanism, Mixed Mode crack-propagation.

1. Introduction.

The pullout test is a non-destructive test procedure which has been suggested by many as an in-place testing procedure alternative to testing field-cast cylinders in the laboratory. The test procedure involves pulling out an anchor plate embedded in concrete with the aid of a tensile jack. During application, a test bolt, consisting of a stem and a circular steel disc, is mounted inside the form (Fig. 1(a)). After curing the concrete, the form is stripped, and the stem is unscrewed. At the time of testing, a rod having a slightly smaller diameter than the stem is screwed into the disc and a cylindrical counterpressure is mounted (Fig. 1(b)). The rod is loaded until failure, where a small piece of concrete can be punched out if sufficient displacement of the rod is applied.

Requirements for the testing configuration are given in ASTM C 900. The embedment depths (that is, the stem length) and head diameter must be equal, but there is no requirement on the magnitude of these dimensions. Commercial inserts have embedment depths about 25 to 30 mm. The inner diameter of the reaction ring can be any size between 2.0 and 2.4 times the insert-head diameter. This means that the apex angle of the conic frustum defined by the insert-head diameter and the inside diameter of the reaction ring (2α in Fig. 1) can vary between 54 and 70 deg. The test apparatus and procedure for the Danish version of the pullout test, the Lok-Test, are illustrated in Fig. 1 [14]. This geometry has been proposed by Kierkegaard-Hansen [11].

The standard pullout test is limited to use in new constructions because the inserts

have to be embedded into fresh concrete. However, other types of pullout test configurations are available for existing constructions [3,4,13,16]. These typically involve drilling a hole and inserting an expanding anchorage device that will engage in the concrete and cause fracture in the concrete when extracted. These techniques are still under development and have not been standardized as ASTM tests methods.

Extensive field investigations on pullout test have been conducted in Europe, Canada, and the United States. A detailed summary on relevant works can be found in Yener and Chen [20]. All laboratory tests indicate that the failure surface is trumpet shaped (Fig. 2). The large diameter of the fragment is determined by the inner diameter of the reaction ring, and the small diameter is determined by the insert-head diameter.

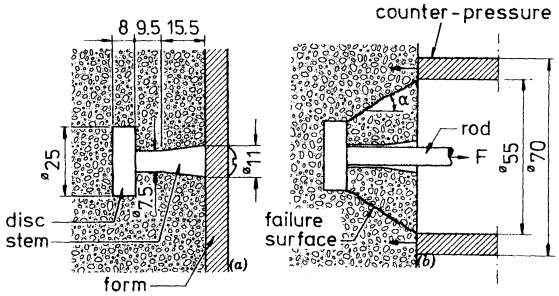

Figure 1: *Application and configuration of Lok-Test (dimensions in millimetres).*

Figure 2: *Shape of the extracted concrete fragment.*

It was found that the pullout force can be linearly related to the compressive strength measured from standard cylinders or cubes [21]. This relationship is not significantly affected by variations in water-cement ratio, type, shape and size of aggregates up to 40 mm maximum aggregate size, type of cement, curing conditions (water cured, cured in air and maltreated), curing time, admixtures, flyash, and air content. Only the use of lightweight aggregates produces a significantly differ correlation [17]. Most of the existing hypotheses seem then to describe the behaviour of concrete in pullout tests through a uniaxial phenomenon. In spite of that, there has been a considerable amount of controversy regarding the property of concrete that is actually measured in pullout tests [21]. It is not clear whether tension, compression, shear, or punching shear strength of concrete is measured, and what constitutes the physical mechanism of failure. Past tests, confirmed by theoretical considerations based on plastic failure of concrete, have shown that the pullout force essentially depends upon compressive strength only for angles $\alpha = 30° \div 35°$ [1]. For angles greater than 45° it depends instead, by a constant of proportionality, mostly upon tensile strength.

2. General remarks on the remeshing CM code.

The theoretical basics of the Cell Method (CM) were developed by Tonti [19]. The essence of the CM is to provide a direct finite formulation of field equations, without requiring a differential formulation.

The main differences between variational formulation and CM are summarized in Ferretti [6]. It will be showed here how heterogeneities do not represent an obstacle with the CM, and how it is possible to easily treat domains with several materials.

The CM uses two meshes, the one the dual of the other. Here, a Delaunay/Voronoi mesh generator [7] is used for analysis in two-dimensional domains (Fig. 3).

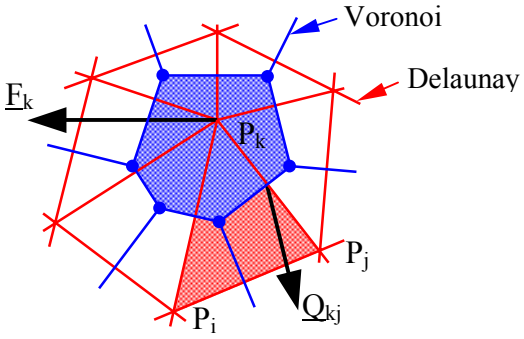

Figure 3: *Mesh of Delaunay/Voronoi*.

In crack propagation problems, the geometry of the mesh must be modified as the crack propagates. The ability of the CM code with remeshing to take a general change in the mesh topology easily into account has been shown by Ferretti [6]. This ability is all the more relevant since

changes in mesh topology are rarely supported by classical finite element method (FEM) numerical codes.

Of the two strategies available for studying fracture mechanics (FM) using the FEM, discontinuity of the stress field and discontinuity of the strain field, the one describing the crack as a displacement discontinuity has been chosen in the CM code with remeshing. For modelling the crack propagation through the mesh, as required by this strategy, the nodal relaxation technique has been adopted. This technique can be achieved using inter-element propagation or intra-element propagation. Inter-element propagation is mesh dependent, since the crack propagates along the mesh side nearest to the computed propagation direction. On the contrary, intra-element propagation is mesh independent, since the crack propagates along the computed propagation direction. This takes more computational time for regenerating the mesh, but leads to more accurate results. The code here employed uses the nodal relaxation with intra-element propagation technique.

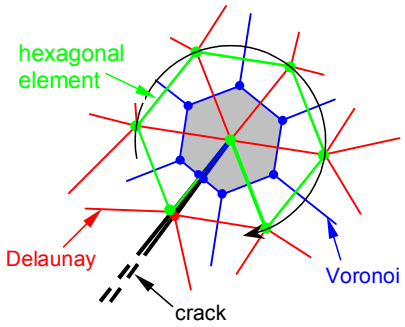

Figure 4: *Element for stress analysis*.

Finally, a special hexagonal element has been studied (Fig. 4), for regularizing the shape of the mesh surrounding the tip. Since the CM associates geometrical objects of the dual mesh to source variables, this regularization allows description of the stress field in a finite neighbourhood of the tip [6]. In the remainder of the domain, the mesh generator is allowed to generate the mesh automatically.

3. Numerical results.

Numerical results concerning the pullout test modelling through the remeshing CM code will be presented here.

Since the dimensions of the concrete specimen are very large in comparison to the dimensions of the steel insert, they can be assumed to be infinite. Because of the axial symmetry (Fig. 5), only one half of the domain has been modelled. Although physically the problem is three-dimensional, the axisymmetry allows mathematical treatment of the problem in two-dimensions.

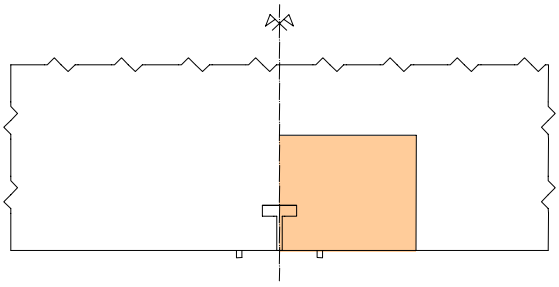

Figure 5: *Geometry to model and stress extinction zone.*

One analysis on the extinction zone has been performed (Fig. 5), in order to identify the minimum finite geometry correctly reproducing the stress-strain field around the steel insert. The minimum finite geometry has been assumed to be square shaped (Fig. 5). This geometry has then been used as modelling domain.

Identification of the unknown boundary conditions.

The pullout test is a typical example of crack propagation in Mixed Mode loading, since the load is applied obliquely both to the crack propagation direction and to the crack opening direction. The combination of loading and boundary conditions forces the edges of the crack to close at some point, where Mode II loading prevails. At the remaining points, the two edges of the crack separate and Mode I loading prevails. Points separating the zones in which Mode I loading prevails from those in which Mode II loading prevails are a function of the load step and crack length. They thus represent an unknown of the Mixed-Mode problem and must be identified before the numerical stress analysis takes place.

Not only the crack edges are subjected to Mixed-Mode loading in the pullout test. Also the surfaces separating the steel insert from the concrete specimen can separate or slide over each other, developing constraint reactions. In this case, the sur-

faces cannot evolve, but the point separating the Mode I loading zone from the Mode II loading zone is still an unknown of the Mixed-Mode loading problem. As has been shown by Ferretti [6], the CM remeshing code is able to automatically estimate which part of the boundary is subjected to Mode I and Mode II loading.

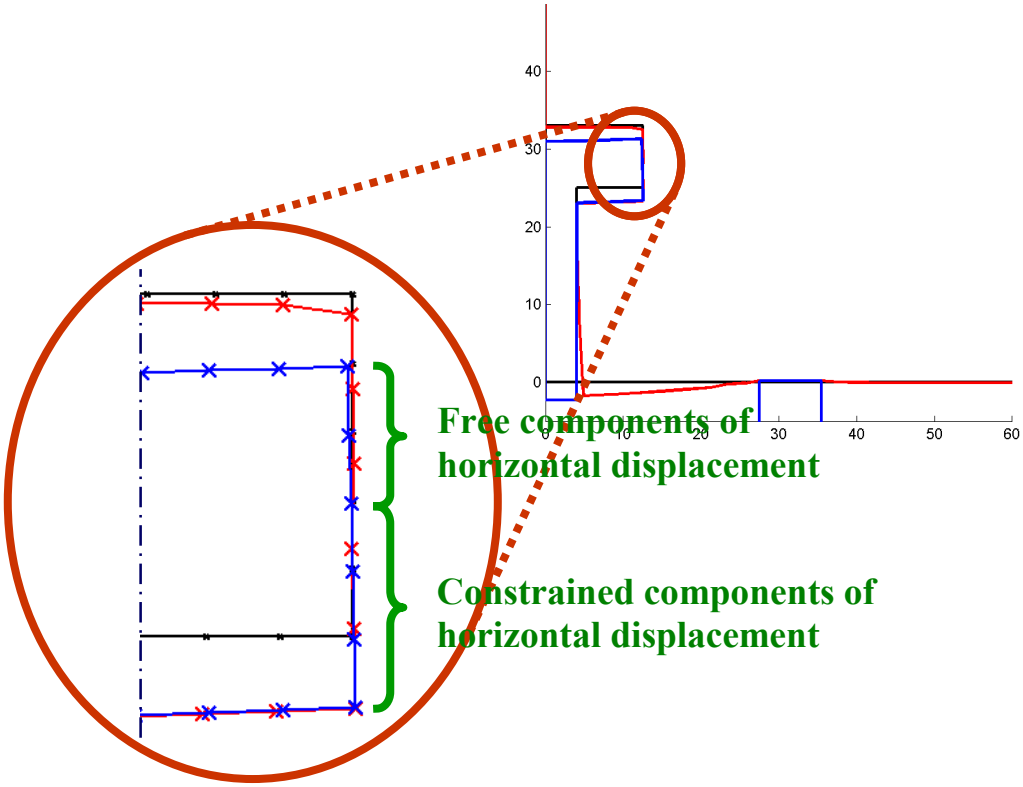

Figure 6: *Detail of the identified boundary conditions on the disk thickness*.

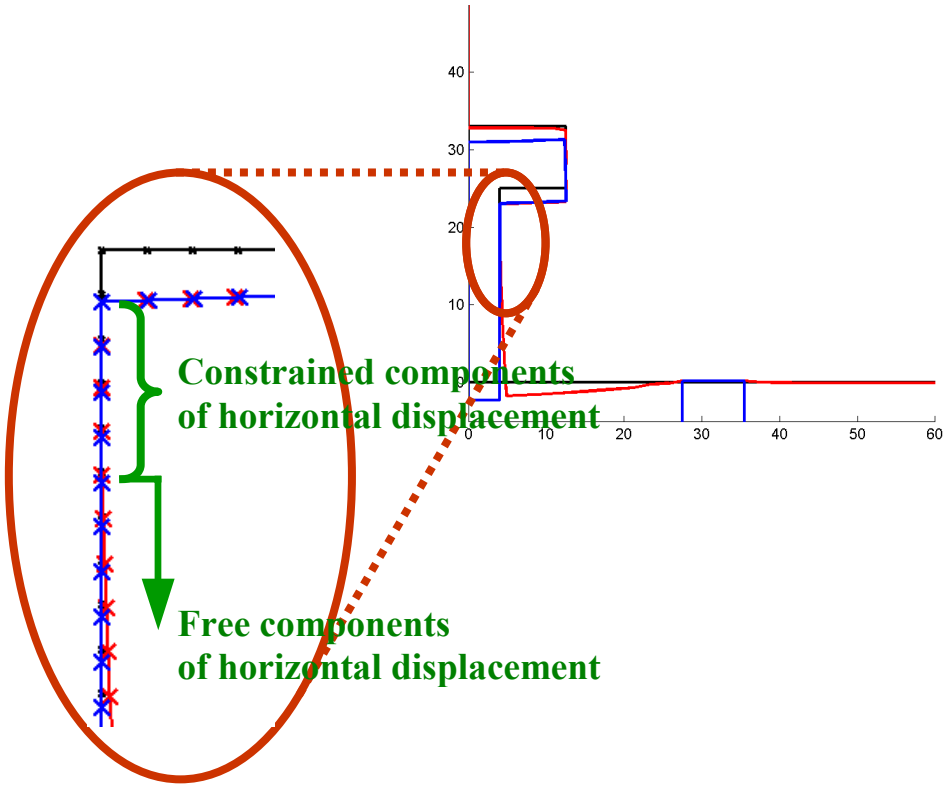

Figure 7: *Detail of the identified boundary conditions on the rod*.

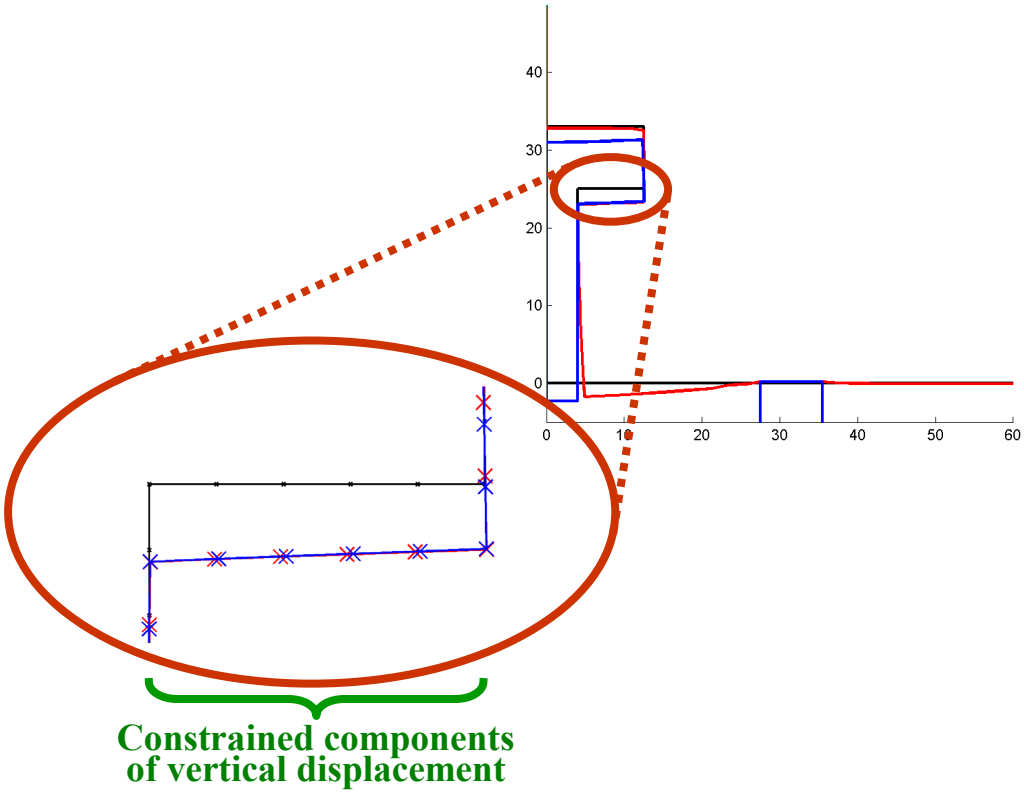

Figure 8: *Detail of the identified boundary conditions on the disk lower edge.*

A friction model has been used there to assess the forces acting across the crack surfaces. This code represents the first case for which a sliding contact problem is solved by means of the CM. It can be considered as the equivalent of the FEM contact elements [8,15,22].

The result of the boundary condition identification on the surfaces separating the steel insert from the concrete specimen is shown in Figs. 6÷8 for the Lok-Test.

Analysis of the stress field.
As previously said, the modelling domain is semi-infinite. The impossibility to operate on a semi-infinite geometry, obliges us to reduce the analysis to the stress extinction zone (Fig. 5).

The simulation has been performed in displacement-control, by imposing the relative displacement between the rod lower edge and the counterpressure ring upper edge. The counterpressure ring has been assumed to be perfectly rigid. It has been considered as an external constraint, and it does not belong to the modelled domain. The zero value of absolute vertical displacements on the external boundary has been fixed on the lower right corner of the extinction zone (assumption of zero displacement at infinity). For this choice, it was possible to estimate the punching effect on the interface between the concrete and the counterpressure ring (Fig. 9).

Figure 9: *Deformed and undeformed configuration at the counterpressure ring.*

The bond between pullout disk and concrete above the disk has been assumed to be monolateral, with the steel nodes free to move downward with regard to the concrete nodes.

In Fig. 10, each Delaunay triangle is provided with a segment, whose direction is that of the principal direction, and whose length is scaled by the principal stress. One can appreciate how the principal stresses approach the zero value on the internal boundary. The principal directions before cracking are shown in Fig. 11, obtained from Fig. 10 by providing each element loaded above a certain value of stress with a segment of fixed length. These directions are quite similar to those

provided by the linear-elastic finite element analysis of Stone and Carino [18].

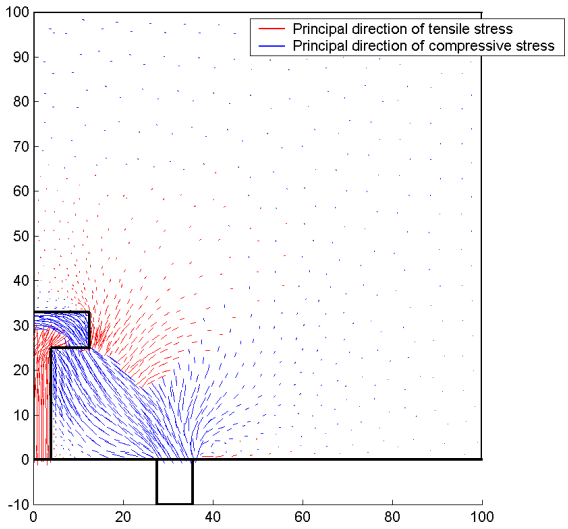

Figure 10: *Numerical principal directions and stresses for the Lok-test.*

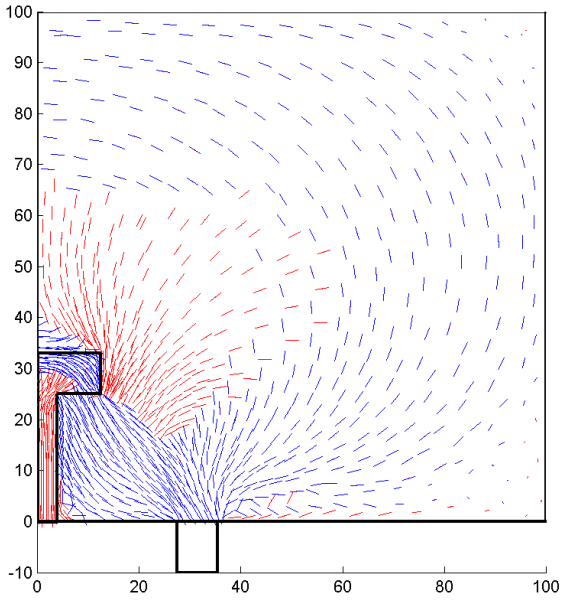

Figure 11: *Tangents to the principal trajectories for Lok-test.*

Moreover, the stress field between the steel insert and the counterpressure ring (Fig. 10) exhibits very large a stress transferring zone of compressive forces.

As will be discussed in the following, the stress transferring zone grows thin as the crack propagates from the disk toward the counterpressure ring. Approaching the ultimate load, a narrow compressed band of stress transferring can be identified, as in the analysis of Ottosen [14]. The large portion of specimen interested by the stress transferring mechanism before cracking is also given by the graphic tool [5] for the stress discrete drawing in the axial direction (Fig. 12). Fig. 12 also shows the pouncing effect on the stress field at the disk-specimen and counter-pressure ring-specimen interfaces.

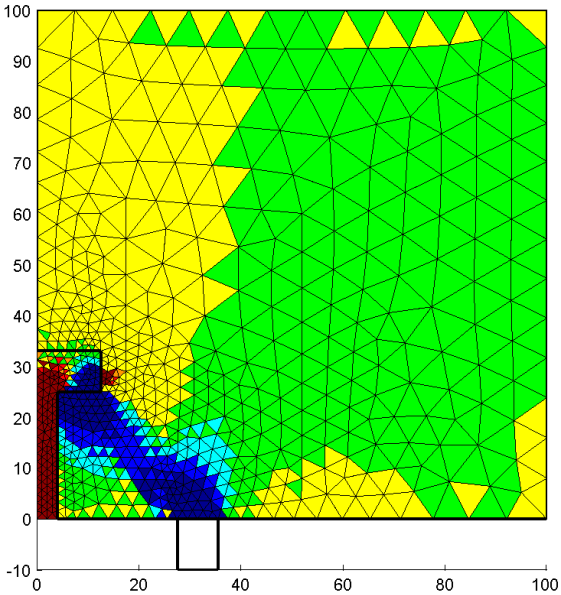

Figure 12: *Discrete stress analysis for the Lok-test.*

The analysis of the stress field is completed by the tool for computing the crack propagation direction proposed by Ferretti [6]. The analysis in the Mohr-Coulomb plane and the crack geometry updating before remeshing activation are the same as in Ferretti [6]. Nevertheless, this second time, the Leon criterion was used:

$$\tau_n^2 = \frac{c}{f_c}\left(\frac{f_{tb}}{f_c} + \sigma_n\right), \qquad (1)$$

where c is the cohesion, f_c the compressive strength, and f_{tb} the tensile strength.

The Leon criterion has been used since the mechanism of failure activation can manifest both in the compressive and tensile fields. The Mohr-Coulomb criterion used by Ferretti [6] is sufficiently adequate for failure mechanisms in the compressive field, while not for failure mechanisms in the tensile field. On the contrary, the Leon criterion is quite adequate both in the compressive and tensile fields.

The two directions of first propagation for the Lok-test are shown in Fig. 13. They

are given by the directions of the lines that join the pole of Mohr to the two tangent points. When the limit condition is reached, both directions activate, and two cracks enucleate. The direction with the minimum slope (in magnitude) with regard to the σ axis was denoted as first direction of propagation, and the direction with the maximum slope (in magnitude) with regard to the σ axis was denoted as second direction of propagation (Fig. 13). Since experimental results show that the propagation along the first direction stops soon after its initiation [12], only the second direction of propagation has been considered in the numerical simulation.

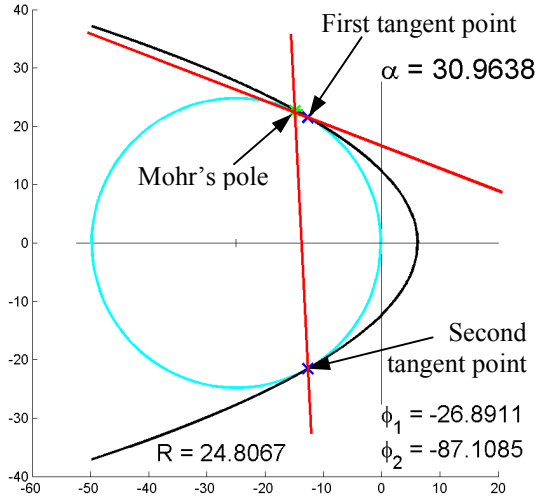

Figure 13: *Limit condition and directions of first propagation for the Lok-Test.*

Analysis of the mechanism of crack initiation.

The experimental results show that the crack initiation mechanism depends on the geometry of the pullout apparatus [2]. In particular, the ratio between the internal diameter of the counterpressure ring and the rod depth is decisive in establishing the type of failure process. That is, the failure mechanism depends on the angle α, defined in Fig. 1. Nevertheless, experimental results are not exhaustive in describing the dependence of the initiation mechanism from α. This leads to the impossibility of identifying a unified model, able to correctly describe the failure mechanism for varying values of α. Such a type of model is of fundamental importance when a numerical analysis based on the equilibrium of the concrete to be extracted is attempted [10]. In this work, the CM remeshing code is proposed as an instrument of analysis, for identifying the correlation between initiation mechanism and α. This is possible since the CM remeshing code operates on both the steel and concrete domains, automatically computing the boundary conditions on the steel-concrete interface. The definition of a steel-concrete behaviour model is not needed and the simplified analysis of equilibrium on the fragment to be extracted is not required. No a-priori assumptions have then been done on the steel-concrete interaction. This last has been identified a-posteriori, as an output of the numerical simulation.

The analysis of the initiation mechanism has been performed in the Mohr-Coulomb plane, with the failure criterion of Leon. As well known, the limit surface of Leon is parabolic (Fig. 13).

The initiation point has been fixed on the right-bottom corner of the disk (Fig. 14), in agreement with experimental [12] and previous numerical results [2,9,14,18,21]. On this point, the special element for stress analysis has been inserted (Fig. 14). The special element used here is a refinement of the special hexagonal element used by Ferretti [6] (Fig. 4), which was studied to be inserted at the crack tip of pre-cracked specimens.

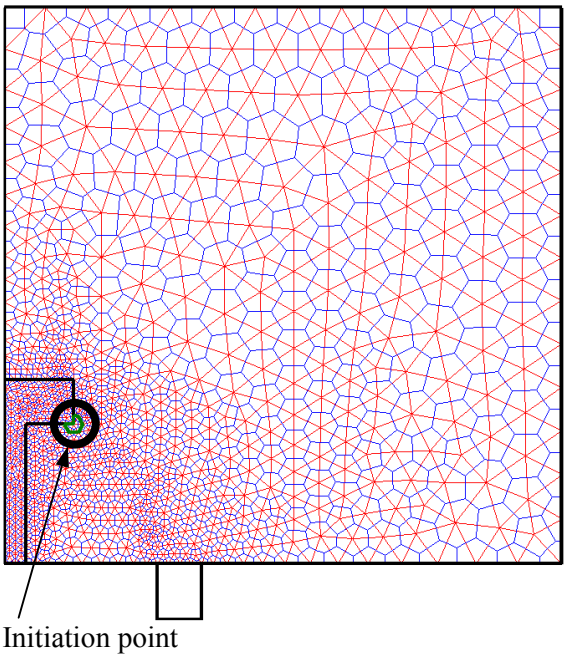

Figure 14: *Meshed domain.*

In Ferretti [6], the specimens were pre-cracked, assuming a crack initiation direction in accordance with the experimental

direction of first propagation. Here, the direction of first propagation is an unknown of the problem, since it is one of the quantities affected by the dependence from α. Consequently, pre-cracking was not possible in the pullout test modelling.

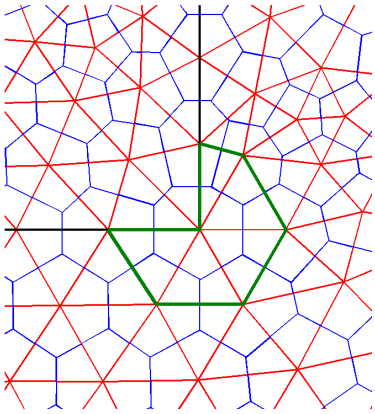

Figure 15: *Element for stress analysis on the domain contour (detail of Fig. 14).*

The special element for stress analysis was then inserted on the known point of initiation, which is a point of the steel-concrete interface. To prevent the special element from intersecting the steel-concrete interface, the geometry of the special element for the first propagation step has been modified as shown in Fig. 15. For further propagation steps, the same hexagonal element as the one used by Ferretti [6] has been inserted at the crack tip.

The mesh generator treats the boundary of the special element as a closed internal interface between two parts of the domain. This leads to specifying a particular mesh geometry in the neighbourhood of the insertion point, with four (five) equilateral triangles. The Voronoi mesh which follows from the special element insertion presents a semi-regular (regular) Voronoi polygon centred on the element insertion point. The association between the sides of this Voronoi cell which are equidistant from the element insertion point and the stress field around the element insertion point itself is shown in Ferretti [6].

The load of crack initiation has been computed from the step-wise identification of the (relative) displacement of crack initiation (simulation in displacement-control). Once the load of crack initiation has been identified, the intersection points between the corresponding Mohr's circle and the limit surface give the mechanism of failure initiation. Figs. 16÷20 provide the Mohr's circle at the limit condition for five values of the angle α. In Fig. 16, the two intersection points lie in the negative semi-plane of the normal stress. Both the corresponding values of shear and normal stresses are not negligible. One can then conclude that the value of the angle α equal to 26.5651° corresponds to a mechanism of failure initiation for shear-compression.

An inspection of Fig. 13 clearly shows that also for the geometry of the Lok-Test ($\alpha = 30.9638°$) the mechanism of failure initiation is for shear-compression. Analogously, one can conclude that the values of the angle α equal to 50.1944°, 63.4349°, 68.1986° and 71.5651° correspond, respectively, to a mechanism of failure initiation for shear-compression (Fig. 17), pure shear (Fig. 18), shear-traction (Fig. 19), and pure traction (Fig. 20).

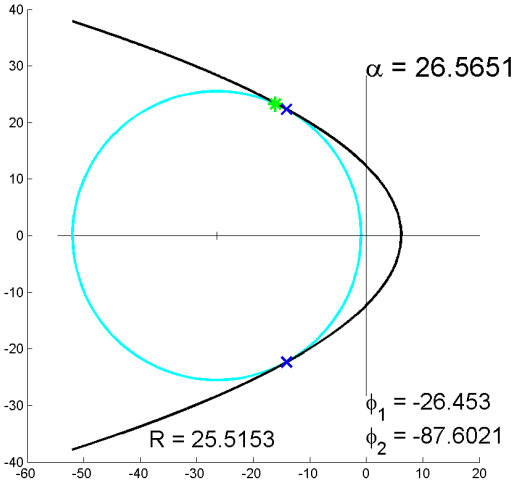

Figure 16: *Limit analysis for* $\alpha = 26.5651$.

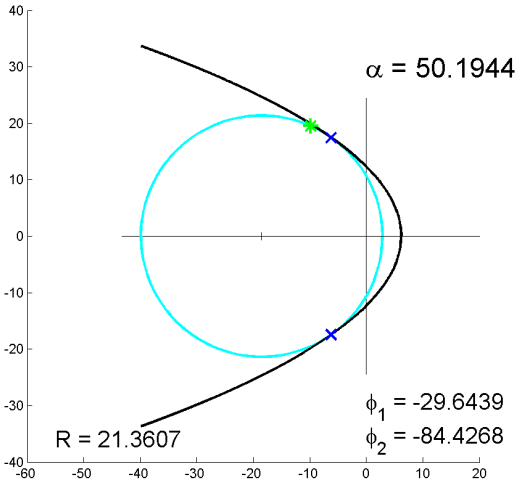

Figure 17: *Limit analysis for* $\alpha = 50.1944$.

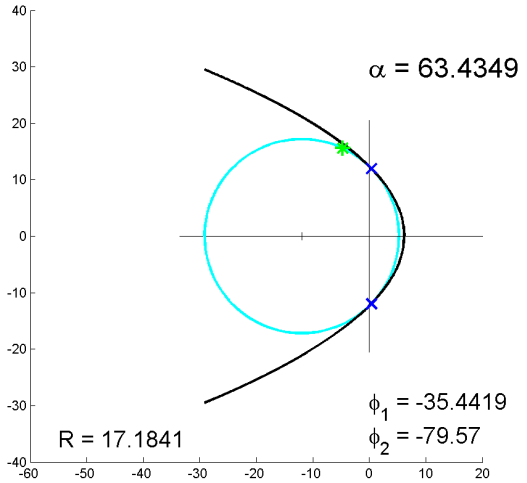

Figure 18: *Limit analysis for* $\alpha = 63.4349$.

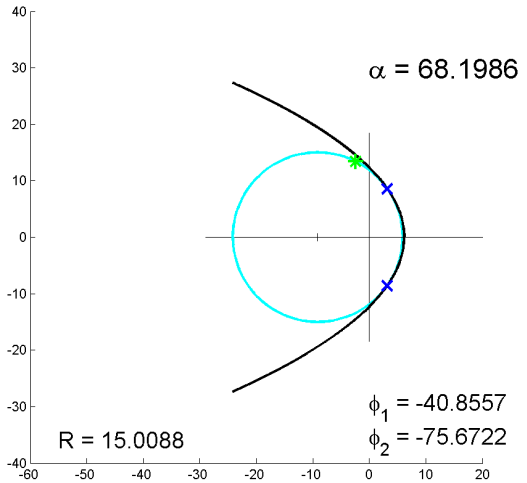

Figure 19: *Limit analysis for* $\alpha = 68.1986$.

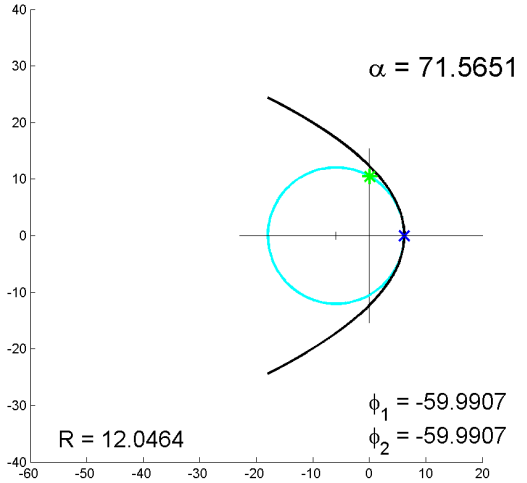

Figure 20: *Limit analysis for* $\alpha = 71.5651$.

The numerical variability with the apex angle, α, of the failure mechanism (Figs. 16÷20) is in good agreement with the findings of the experimental programme of Bocca, Carpinteri and Valente [2].

Values of first propagation for varying diameter of the counterpressure ring

The radius of Mohr, the directions of first propagation, the load of first propagation, and the displacement of first propagation are given in Figs. 21÷24 for the angle α varying from the lower limit required by ASTM C 900 ($27 \le \alpha \le 35$) and the upper limit of the experimental programme of Bocca, Carpinteri and Valente (1989) ($20.5 \le \alpha \le 71.5$). The filled in regions in Figs. 21÷24 correspond to the ASTM C 900 requirements for α. The radius of Mohr, the first angle of first propagation, and the load of first propagation are decreasing with α. The second angle of first propagation, lower than the first angle of first propagation, is increasing with α, and equals the first angle of first propagation from the value of α corresponding to the mechanism of pure traction on ($\alpha \cong 71°$). Actually, when the failure mechanism is of pure traction, the two intersection points and the two propagation direction, coincide (Fig. 20). Finally, the displacement of first propagation is decreasing in the ASTM C 900 range of α. Then, it reaches a minimum for a value of α of about 38°. For greater values of α, the displacement of first propagation increases, reaching a maximum for the failure mechanism of pure shear ($\alpha \cong 63°$). From this point on, the behaviour is decreasing with the angle α again.

Crack propagation analysis.

A step-wise analysis of crack propagation has been performed for the Lok-Test.

The numerical crack path and the stress analysis predicted by the numerical model are shown in Fig. 25 for the final failure stage. In accordance with the experimental results (Fig. 2), the numerical direction of propagation changes at every stage. In particular, after a sub-vertical propagation the propagation direction changes abruptly and the crack propagates towards the counterpressure ring. The intra-element propagation technique and reduction of the mesh size near the crack tip allow the crack path to be accurately predicted.

From comparison between Figs. 12 and 25, one can conclude that the static scheme of the resistant structure changes at each propagation step. At first, the resistant structure is subjected to compressive stresses along the disk-counterpressure

ring direction. For this stage, the principal stresses are nonuniform and the principal directions are not parallel to each other, as in the linear-elastic finite element analysis of Stone and Carino [18]. As the crack propagates, bending actions superimpose to the compressive stresses. As a consequence, the transferring zone of compressive stresses becomes thinner and thinner, and the non-uniform stress behaviour is enhanced. Comparison of a neutral axis in the fragment to be extracted arises simultaneously to the change of crack propagation direction, leading to a tension zone near the stem. During the latter stages of crack propagation the bending actions become dominant. It can than be concluded that crack propagation also involves progressive bending of the compressed concrete within the concrete to be extracted. This result agrees with the plastic-fracture finite element analysis of Yener [21].

A tensile state of stress with principal direction perpendicular to last edge of the crack arises when the direction of crack propagation changes. Since the crack direction will remain unchanged from this moment forth, it is reasonable to conclude that the tensile state of stress contributes to crack propagation in the last stage of the pullout test. Also opening of the crack edges behind the crack tip confirms this assumption (Fig. 25).

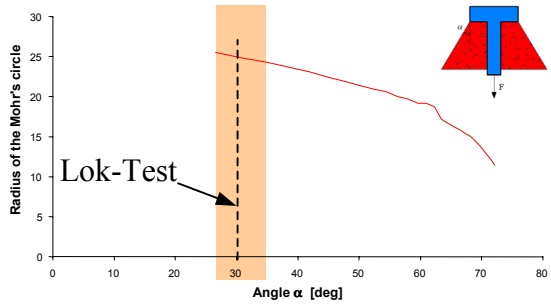

Figure 21: *Mohr radius at crack initiation versus the apex angle.*

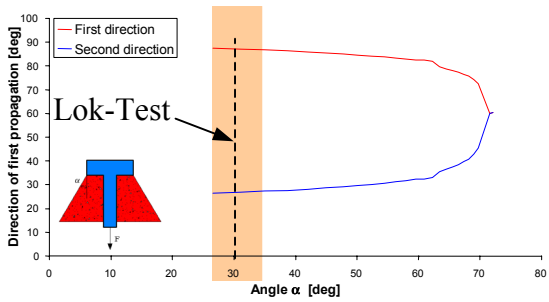

Figure 22: *Propagation directions at crack initiation versus the apex angle.*

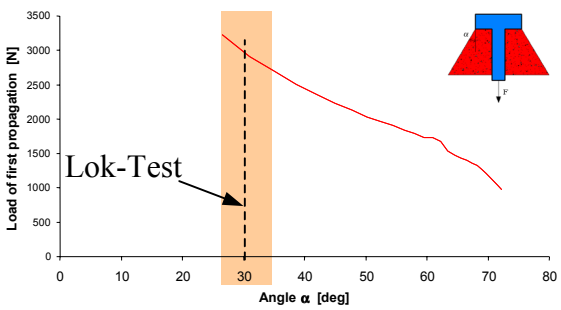

Figure 23: *Load at crack initiation versus the apex angle.*

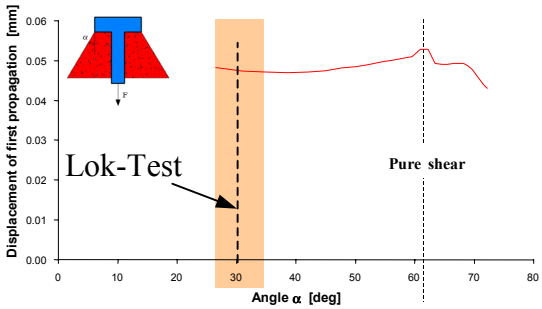

Figure 24: *Displacement at crack initiation versus the apex angle.*

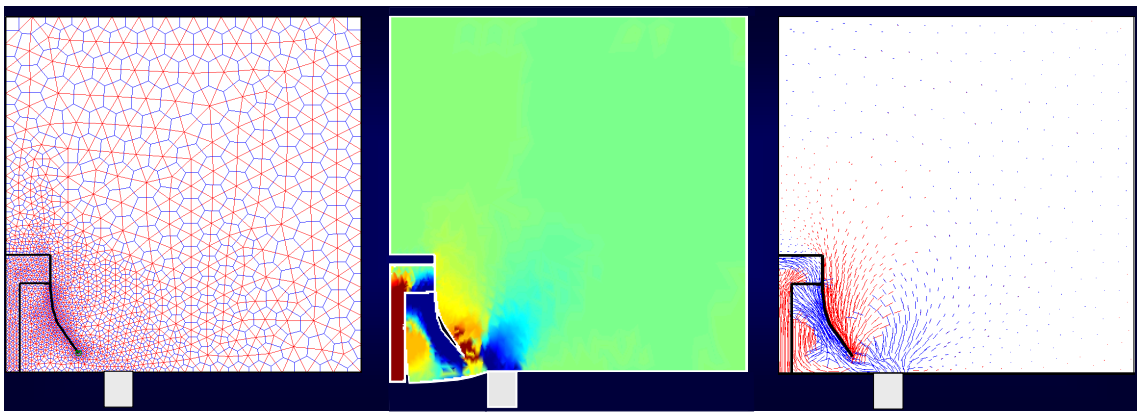

Figure 25: Mesh, stress and strain analysis for the final failure stage (Lok-Test).

In Fig. 26, the zoom of the deformed steel disk is provided at the upper interface between steel and concrete, soon before the crack starts to propagate. As in Yener [21], the steel disk bends pronouncedly, while the concrete is quite undeformed. At this point, the concrete within the eventual failure surface is compressed along the insert-support ring direction. When the crack activates, the decrease of concrete stiffness under the steel disk due to crack propagation leads to a disk bending close to zero (Fig. 27). From this moment forth, the stiffness of the steel disk can be assumed to be infinite.

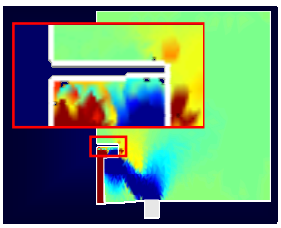

Figure 26: *Deformed configuration above the disk shortly before crack initiation.*

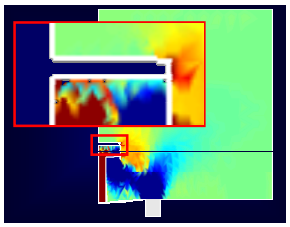

Figure 27: *Deformed configuration above the disk soon after crack initiation.*

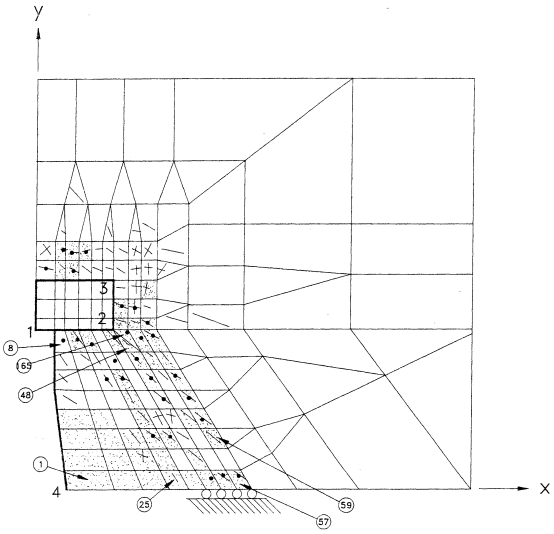

Figure 28: *Finite element mesh and predicted failure in the plastic-fracture finite element analysis performed by Yener [21].*

With reference to the node numeration in Fig. 28, the followings are further similarities between the present and the plastic-fracture finite element analysis performed by Yener [21]:-

- The vertical downward displacement of node 1, δ_1 is always greater than that of node 2, δ_2.
- Both δ_1 and δ_2 are always greater than δ_4.
- The concrete to be extracted pushes against the main body of the concrete near the support ring and against the steel stem near point 1.
- High compressive interacion exists between the stem and the concrete direcly below the steel disk in the vicinity of the periphery near to point 1.

4. Conclusions

A CM code has been used here both for crack initiation and crack propagation analysis in the pullout test modelling. Several ratios between the internal diameter of the counterpressure ring and the rod length have been taken into account for the crack initiation analysis. The crack propagation analysis has been performed for the geometry of the Lok-Test. The adopted CM code combines nodal relaxation, intra-element propagation and remeshing. It also permits the mesh dimensions to be refined at specific locations, so as to improve the accuracy of the solution. The ability of the mesh generator to operate on multiple domains has been used to provide the evolving stress field both in the steel insert and concrete specimen. Finally, the code automatically estimates which part of the boundary is subjected to Mode I loading, and which part is subjected to Mode II loading. Consequently, no a-priori assumptions are needed on the steel-concrete interaction. The computation is then performed on the whole domain, without having to reduce the analysis on the equilibrium condition of the extracted concrete. The simulation is displacement-controlled.

The agreement between the CM results and the results of previous FEM analysis further states that the CM can give good

predictions for fracture mechanics problems. Also the experimental results are well reproduced.

The step-wise analysis of the state of stress allows us to describe the progressive failure of the concrete medium. It was found that the crack initiation mechanism depends upon the ratio between the internal diameter of the counterpressure ring and the rod length. A changing in the crack initiation mechanism from shear-compression to shear-tension was found to occur for the angle α equal to about 63°.

Moreover, the crack propagation mechanism changes as the crack propagates. At first, the concrete between the steel disk and the counterpressure ring is compressed in the disk-ring direction. Subsequently, bending actions develop in the concrete fragment to be extracted. They become more and more relevant with the evolving of the failure process and a neutral axis arises in the concrete fragment. Compressive interactions between steel rod and concrete specimen and the punching effect at the disk-concrete interface cause the neutral axis to intersect the rod-concrete interface, never arriving at the disk-concrete interface. The direction of the neutral axis is more or less parallel to the crack direction. The comparison of the neutral axis seems to be correlated to the abrupt change of the crack propagation direction, also experimentally observed. From the moment in which the crack direction changes on, a tensile state of stress develops in front of the crack tip. It may then be reasonable to assume that tensile strength of the concrete has some kind of indirect influence on the pullout strength.

It can be concluded that it may be not appropriate to describe the complex state of stress induced in pullout test by a uniaxial mode of failure. As in the conclusions of the linear-elastic finite element analysis of Stone and Carino, it can also be asserted that an alternative explanation needs to be found for the experimentally observed close correlation between compressive and pullout strength.

The analysis of the stress field provides a detailed description of the stress redistribution with the crack propagation. It seems then that the CM code is able to provide a substantial contribution to the comprehension of the physical mechanism of failure in pullout tests.

The analysis performed has been carried out by following only one of the two experimentally observed crack paths. Numerical results can improve if the second crack path is modelled as well. Further studies are currently being undertaken to activate the second propagation and study the mutual influence between the two cracks. Moreover, an extension of the code in such a way as to take into account the friction between the nodes lying on the crack edges is being studied at the present time. Finally, also combination of concrete crushing and concrete cracking is under study at the moment, so as to derive the complete load-displacement diagram in pullout tests.

Acknowledgements
All the results here presented are part of the CIMEST Scientific Research on the Identification of Materials and Structures – DISTART – Faculty of Engineering – Alma Mater of Bologna.

References

[1] Bocca, P. (1984), *Matériaux et Constructions*, **17**, No. 99, pp. 211-216.

[2] Bocca, P., Carpinteri, A., Valente, S. (1989), *Fracture of Concrete and Rock*, pp. 347-356.

[3] Chabowski, A. J., Bryden-Smith, D. W. (1980), *Mag Concrete Res*, **32**, No. 112, pp. 164-172.

[4] Domone, P. L., Castro, P. F. (1987), *Proc. Structural Faults and Repairs 87*.

[5] Ferretti, E. (2001), *Modellazione del Comportamento del Solido Cilindrico Compresso*, Ph.D. Thesis, University of Lecce, Italy.

[6] Ferretti, E. (2003), *CMES*, **4**, No. 1, pp. 51-72.

[7] George, P. L. (1995), *Surv Math Ind*, pp. 239-247.

[8] Har, J. (1998), *Ph.D. Thesis*, Georgia Institute of Technology, Atlanta.

[9] Hellier, A. K, Sansalone, M., Carino, N. J., Stone, W. C., Ingraffea, A. R. (1987), *Journal of Cement, Concrete and Aggregates*, **9**, No. 1, pp. 20-29.

[10]Jensen, B. C., Bræstrup, M. W. (1976), *Nordisk Betong (Journal of the Nordic Concrete Federation)*, No. 2, pp. 9-11.

[11] Kierkegaard-Hansen, P. (1975), *Nordisk Betong (Journal of the Nordic Concrete Federation)*, No. 3, pp. 19-28.

[12] Krenchel, H., Bickley, J. A. (1985), *Nordic Concrete Research*, No. 6, The Nordic Concrete Federation.

[13] Mailhot, G., Bisaillon, G., Carette, G. G., Malhotra, V. M. (1979), *ACI Journal*, **76**, No. 12, pp. 1267-1282.

[14] Ottosen, N. S. (1981), *Journal of the Structural Division*, **107**, No. ST4, pp. 591-603.

[15] Papadopoulos, P., Jones, R. E., Solberg, J. (1995), *Int J Num Meth Engrg*, **38**, pp. 2603-2617.

[16] Petersen, C. G. (1984), Proceedings, Institution of Civil Engineering, Part I, **76**, pp. 539-549.

[17] Petersen, C. G. (1997), Proc. Non-Destructive Testing in Civil Engineering Conference, pp. 1-10.

[18] Stone, W. C., Carino, N. J. (1984), *ACI Journal*, **81**, No. 1, pp. 3-12.

[19] Tonti, E., (2001), *CMES*, **2**, No. 2, pp. 237-258.

[20] Yener, M., Chen, W. F. (1984), *Journal of Cement, Concrete, and Aggregates*, **6**, No. 2, pp. 90-99.

[21] Yener, M. (1994), *ACI Structural Journal*, **91**, No. 1, pp. 49-58.

[22] Zhong, Z. H. (1993), *Finite Element Procedures for Contact-Impact Problems*, Oxford/New York/Tokyo, 372 pp.